Finite-size effects on active chaotic advection

Takashi Nishikawa
Department of Mathematics, Arizona State University, Tempe, Arizona 85287

Zoltán Toroczkai
Theoretical Division and Center for Nonlinear Studies, Los Alamos National Laboratory, Mail Stop B258, Los Alamos, New Mexico 87545

Celso Grebogi
Instituto de Física, Universidade de São Paulo, Caixa Postal 66318, 05315-970, São Paulo, SP, Brazil

Tamás Tél
Institute for Theoretical Physics, Eötvös University, P.O. Box 32, H-1518, Budapest, Hungary
(Received 30 July 2001; published 24 January 2002)

A small (but finite-size) spherical particle advected by fluid flows obeys equations of motion that are inherently dissipative, due to the Stokes drag. The dynamics of the advected particle can be chaotic even with a flow field that is simply time periodic. Similar to the case of ideal tracers, whose dynamics is Hamiltonian, chemical or biological activity involving such particles can be analyzed using the theory of chaotic dynamics. Using the example of an autocatalytic reaction, $A+B\rightarrow 2B$, we show that the balance between *dissipation* in the particle dynamics and *production* due to reaction leads to a steady state distribution of the reagent. We also show that, in the case of coalescence reaction, $B+B\rightarrow B$, the decay of the particle density obeys a universal scaling law as approximately t^{-1} and that the particle distribution becomes restricted to a subset with fractal dimension D_2, where D_2 is the correlation dimension of the chaotic attractor in the particle dynamics.

DOI: 10.1103/PhysRevE.65.026216 PACS number(s): 05.45.−a, 47.70.Fw, 87.23.Cc

I. INTRODUCTION

Active processes under chaotic advection, such as the dynamics of growing population of plankton or evolving distribution of active chemicals in environmental flows, have attracted significant amount of attention in recent years [1–13]. These previous studies have shown that the chaotic saddle for the Lagrangian dynamics in the open flows can act as a catalyst for the chemical reaction or biological reproduction. The theory of chaotic dynamics was used to show that this catalytic effect, due to the fractality of the chaotic saddle and its unstable manifold, introduces a term in the equation for the reaction kinematics that depends on the chaotic properties of the Lagrangian dynamics.

In these studies, however, the particles were assumed to be point particles without mass, which traces a fluid element perfectly. This assumption, of course, is an oversimplification of the reality—especially when the biological activity of concern is such as that of a plankton population. A more realistic assumption would be that of a spherical particle that is small, but it has finite size, and it is subject to the forces exerted by the fluid surrounding it. The equations of motion for such particles were derived by Maxey [14] for low Reynolds number, and they include terms representing not only the Stokes drag force and buoyancy force, but also the added mass effect, Basset history effect, and the Faxen corrections. Even in the situation where the Basset history term and the Faxen corrections can be ignored, the dynamics of the particle is strikingly different from the case of a point particle without mass. While the dynamics of an ideal tracer in an incompressible, stationary n-dimensional flow is area preserving in its n-dimensional phase space, the dynamics of a small particle in the same flow is contracting in its $2n$-dimensional phase space. In other words, the dynamics of finite size particles is *dissipative*.

In this paper, we choose the two-dimensional oscillating cellular vortex flow field represented by a simple stream function ψ:

$$\psi(\mathbf{Y},t)=\frac{U_0 L}{\pi}(1+k\sin\omega t)\sin\frac{\pi Y_1}{L}\sin\frac{\pi Y_2}{L}, \qquad (1)$$

where $\mathbf{Y}=(Y_1,Y_2)$ is the position, L is the size of a vortex cell, and U_0 gives the maximum velocity of the flow field for $k=0$. Figure 1 shows the streamlines, or the contour plot of the stream function in Eq. (1) as solid curves. The time-independent version of the same flow field was extensively studied by Maxey [15], in which it was found that the particles subjected to such flow field converge asymptotically either to an equilibrium point or to a smooth curve extending through the vortex cells. To model more realistic situations, we impose a simple periodic time dependence in the stream function by varying the vorticity of each vortex sinusoidally. It turns out that such a simple time dependence can make the dynamics of a small particle much more interesting although the motion of pointlike tracers would still follow the streamlines of Eq. (1). We find that for certain range of parameter values, the asymptotic behavior of a small particle of finite size can even be chaotic and exhibit an attractor whose projection onto the physical coordinate space is a fractal set. Such a situation is shown in Fig. 1.

The goal of this paper is to show that such fractal attractors in the coordinate space also act as catalysts for the reaction, just as in the case of ideal tracers, even though the

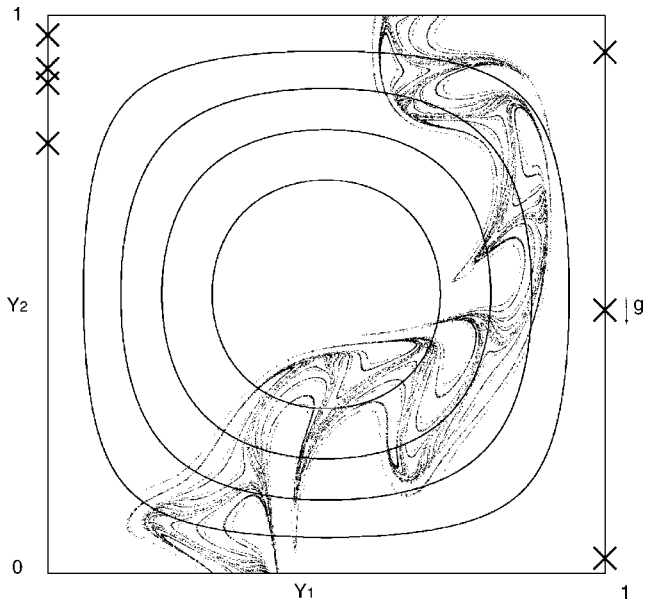

FIG. 1. Trajectories on the chaotic (dots) and the period 7 (crosses) attractors of the stroboscopic map $\tilde{F}$ with $A=3.2$, $R=1$, $W=0.8$, $k=2.72$. In the background, level curves of the stream function in Eq. (1) are plotted for reference. The gravity **g** points downward, and trajectories move up on average because particles are lighter than the surrounding fluid.

dynamics of the particles is qualitatively different. The key element is to replace the escape rate from a chaotic saddle along its unstable manifold for the case of ideal tracers with the smallest average contraction rate on the attractor in this case. However, things are not as simple because the particle dynamics can have multiple attractors, as is the case with the flow field we are considering.

This paper is organized as follows. In Sec. II, we give the equation of motion for a small spherical particle in the oscillating cellular vortex flow field, and introduce the associated discrete dynamical system for later analysis. In Sec. II, we discuss the attractors for the dynamics, along with the mechanism of their births. In Sec. IV, we give detail of the implementation of our model system. In Sec. V, we consider the reaction of autocatalytic type, $A+B\rightarrow 2B$, with continuous feeding of the reagent B. In Sec. VI, we consider the reaction in closed system, to analyze the asymptotic reagent distribution. Finally, in Sec. VII, we discuss the coalescence type of reaction, $B+B\rightarrow B$, and Sec. VIII is reserved for conclusions.

II. EQUATION OF MOTION

We consider the motion of a small, spherical particle in the flow field of an infinite array of cellular vortices as discussed by Maxey [15], but with a time dependence to allow for a nontrivial chaotic behavior. The flow is two dimensional, incompressible, and time periodic, and is represented by the stream function in Eq. (1). Notice that the introduction of a simple periodicity in time, as the factor $(1+k\sin\omega t)$, does not change the streamlines. Yu, Grebogi, and Ott [16] obtained the equations of motion for a particle in the flow field defined by Eq. (1), but we will briefly go through the derivation here for completeness.

We follow the derivation of Maxey in [15], except that the time dependence of the flow field is taken into account. The equation of motion for the dynamics of a small rigid spherical particle with radius a [14] is

$$m_p\frac{d\mathbf{V}}{dt}=(m_p-m_F)\mathbf{g}+m_F\left.\frac{D\mathbf{u}}{Dt}\right|_{\mathbf{Y}(t)}-\frac{1}{2}m_F\frac{d}{dt}\left(\mathbf{V}-\mathbf{u}(\mathbf{Y},t)-\frac{1}{10}a^2\nabla^2\mathbf{u}\right)-6\pi a\mu\mathbf{X}(t)-6\pi a^2\mu\int_0^t d\tau\frac{d\mathbf{X}(\tau)/d\tau}{\sqrt{\pi\nu(t-\tau)}},\tag{2}$$

where

$$\mathbf{X}(t)=\mathbf{V}(t)-\mathbf{u}(\mathbf{Y}(t),t)-\tfrac{1}{6}a^2\nabla^2\mathbf{u},$$

$\mathbf{Y}(t)$ and $\mathbf{V}(t)$ are the position and velocity of the particle respectively, $\mathbf{u}(\mathbf{Y},t)$ is the flow field in the position $\mathbf{Y}$ of the particle at time t. Here m_p is the mass of the particle, m_F is the mass of the displaced fluid, and ν is the kinematic viscosity. The term $m_F(Du/Dt)|_{\mathbf{Y}(t)}$ is the acceleration of the fluid element in the position $\mathbf{Y}(t)$ at time t and represents the force exerted on the particle by the surrounding fluid. Since the particle is not an ideal tracer, it is important to distinguish between the Lagrangian derivative

$$\frac{D\mathbf{u}}{Dt}=\frac{\partial\mathbf{u}}{\partial t}+\mathbf{u}\cdot\nabla\mathbf{u}$$

taken along the trajectory of a fluid element and

$$\frac{d\mathbf{u}}{dt}=\frac{\partial\mathbf{u}}{\partial t}+\mathbf{V}\cdot\nabla\mathbf{u}$$

taken along the trajectory of the particle. The term $(m_p-m_F)\mathbf{g}$ is the buoyancy force, the term

$$-\frac{1}{2}m_F\frac{d}{dt}\left(\mathbf{V}-\mathbf{u}-\frac{1}{10}a^2\nabla^2\mathbf{u}\right)$$

represents the added mass effect, the term $-6\pi a\mu\mathbf{X}(t)$ is the Stokes drag force,

$$-6\pi a^2\mu\int_0^l d\tau\frac{d\mathbf{X}/d\tau}{\sqrt{\pi\nu(t-\tau)}}$$

is called the Basset history term, and the terms involving $a^2\nabla^2\mathbf{u}$ are the so-called Faxen corrections for the nonuniform flow field. Equation (2) is valid for small particles at low Reynolds numbers of up to about 250.

It was pointed out by Auton, Hunt, and Prud'homme [17] that the correct form of the added mass term should be

$$-\frac{1}{2}m_F\left[\frac{d\mathbf{V}}{dt}-\frac{D}{Dt}\left(\mathbf{u}-\frac{1}{10}a^2\nabla^2\mathbf{u}\right)\right].$$

This correction, as mentioned in [14], is small for low Reynolds number, and hence would not change the qualitative results to be described below.

In the case of the flow field represented by the stream function (1), the Faxen corrections simplify as

$$a^2\nabla^2\mathbf{u}=-\frac{2a^2\mathbf{u}}{L^2},$$

so the effect in the Eq. (2) is equivalent to decreasing $\mathbf{u}$ by a small amount $\sim(a/L)^2$. Thus, the correction is unlikely to affect the qualitative behavior of the system and we neglect these terms in Eq. (2). The Basset history term is also neglected since it can be shown [18] that if the fluid inertia effect is included, then the Basset history term is less significant than the other terms. Taking these into account, the equation of motion for the particles in the time periodic cellular flow field (1) is

$$\left(m_p+\frac{m_F}{2}\right)\frac{d\mathbf{V}(t)}{dt}=(m_p-m_F)\mathbf{g}+6\pi a\mu[\mathbf{u}(\mathbf{Y},t)-\mathbf{V}]+m_F\mathbf{u}\cdot\boldsymbol{\nabla}\mathbf{u}+\frac{1}{2}m_F\mathbf{V}\cdot\boldsymbol{\nabla}\mathbf{u}+\frac{3}{2}m_F\frac{\partial\mathbf{u}}{\partial t},$$

which only differs from the one in [15] by the last term. After making the variables dimensionless by

$$\mathbf{Y}^*=\frac{\mathbf{Y}}{L},\quad \mathbf{V}^*=\frac{\mathbf{V}}{U_0}\quad \mathbf{u}^*=\frac{\mathbf{u}}{U_0},\quad t^*=\frac{tU_0}{L},$$

and suppressing the asterisks, we get

$$\frac{d\mathbf{V}(t)}{dt}=A[\mathbf{u}(\mathbf{Y},t)-\mathbf{V}+\mathbf{W}]+R\left(\mathbf{u}+\frac{1}{2}\mathbf{V}\right)\cdot\boldsymbol{\nabla}\mathbf{u}+\frac{3}{2}R\frac{\partial\mathbf{u}}{\partial t},\tag{3}$$

where

$$A=\frac{6\pi a\mu L}{(m_p+\frac{1}{2}m_F)U_0},\quad R=\frac{m_F}{m_p+\frac{1}{2}m_F},$$

and

$$\mathbf{W}=\frac{m_p-m_F}{6\pi apU_0}\mathbf{g}.$$

The parameter A represents the amount of damping, or the effect of the inertia of the particle. The limit of $A\to\infty$ corresponds to the case of point particles with no inertia (since m_F and m_P are proportional to a^3). R is the mass ratio parameter and $R<\frac{2}{3}$ corresponds to aerosols (heavier than the fluid), and $R>\frac{2}{3}$ corresponds to bubbles (lighter than the fluid). $\mathbf{W}$ is the scaled particle settling velocity for still fluid. The dimensionless stream function is

$$\psi^*(\mathbf{Y},t)=\frac{1}{\pi}(1+k\sin\omega^*t^*)\sin\pi Y_1^*\sin\pi Y_2^*,$$

where

$$\omega^*=\frac{\omega L}{U_0},$$

so, the dimensionless velocity field, after suppressing the asterisks, is

$$\mathbf{u}(\mathbf{Y},t)=\begin{pmatrix}\dfrac{\partial\psi(\mathbf{Y},t)}{\partial Y_2}\\ -\dfrac{\partial\psi(\mathbf{Y},t)}{\partial Y_1}\end{pmatrix}=\begin{pmatrix}(1+k\sin\omega t)\sin\pi Y_1\cos\pi Y_2\\ -(1+k\sin\omega t)\cos\pi Y_1\sin\pi Y_2\end{pmatrix}.$$

By plugging this into Eq. (3), we get the full equations of motion

$$\frac{dY_1}{dt}=V_1,\tag{4}$$

$$\frac{dY_2}{dt}=V_2,\tag{5}$$

$$\begin{aligned}\frac{dV_1}{dt}=&-AV_1+A(1+k\sin\omega t)\sin\pi Y_1\cos\pi Y_2\\&+\frac{R}{2}(1+k\sin\omega t)(V_1\cos\pi Y_1\cos\pi Y_2\\&-V_2\sin\pi Y_1\sin\pi Y_2)+R(1+k\sin\omega t)^2\\&\times\sin\pi Y_1\cos\pi Y_1+\frac{3R}{2}\omega k\cos\omega t\\&\times\sin\pi Y_1\cos\pi Y_2,\end{aligned}\tag{6}$$

$$\begin{aligned}\frac{dV_2}{dt}=&-AV_2-A(1+k\sin\omega t)\cos\pi Y_1\sin\pi Y_2+AW\\&+\frac{R}{2}(1+k\sin\omega t)(V_1\sin\pi Y_1\sin\pi Y_2\\&-V_2\cos\pi Y_1\cos\pi Y_2)+R(1+k\sin\omega t)^2\\&\times\sin\pi Y_1\cos\pi Y_2-\frac{3R}{2}\omega k\cos\omega t\\&\times\cos\pi Y_1\sin\pi Y_2.\end{aligned}\tag{7}$$

One can see that the Maxey equation is immediately recovered for $k=0$.

The terms $-AV_1$ and $-AV_2$ in the equations indicate that the flow defined by Eqs. (4)–(7) in the phase space is dissipative. A straightforward calculation shows that the divergence of the flow in the phase space is $-2A$, so a volume

element in the phase space $\mathbf{R}^4$ shrinks exponentially under the flow as e^{-2At}. Note that in the limit $A\to\infty$, where the dissipation is infinitely fast, one can see from Eq. (3) that the flow dynamics collapses onto the two-dimensional surface defined by $\mathbf{V}=\mathbf{u}(\mathbf{Y},t)+\mathbf{W}$ in the phase space. The projection of this dynamics onto the $\mathbf{Y}$-coordinate space is volume preserving, because the fluid flow is incompressible, and it corresponds to the dynamics of ideal tracers without any inertia effect. The goal of this paper is to investigate the effect of the dissipation on the reaction dynamics.

Since the system (4)–(7) describing the particle dynamics is a periodically forced system, it is natural to consider the stroboscopic section defined by the time-T map of the flow, where T is the period of the flow. We denote this map by F. It is easy to check that if $(Y_1(t),Y_2(t),V_1(t),V_2(t))^T$ (T denotes transpose) is a solution of Eqs. (4)–(7), then

$$\begin{pmatrix} Y_1(t)+2n \\ Y_2(t)+2m \\ V_1(t) \\ V_2(t) \end{pmatrix}, \quad \begin{pmatrix} Y_1(t)+1 \\ Y_2(t)+1 \\ V_1(t) \\ V_2(t) \end{pmatrix},$$

$$\begin{pmatrix} 2-Y_1(t) \\ Y_2(t) \\ -V_1(t) \\ V_2(t) \end{pmatrix}, \quad \begin{pmatrix} 1-Y_1(t) \\ Y_2(t)+1 \\ -V_1(t) \\ V_2(t) \end{pmatrix}$$

are also solutions, where m,n are integers. After identifying all these points with $(Y_1(t),Y_2(t),V_1(t),V_2(t))^T$, the mapping F can be regarded as being defined on $E=[0,1]\times[0,1]\times\mathbf{R}^2$ ($\mathbf{R}^2$ are the velocity components). We denote this mapping by $\tilde{F}$, in order to distinguish it from F defined on the whole phase space. In fact, the original dynamics represented by Eqs. (4)–(7) can also be defined on E, by reflecting everything about $Y_1=1/2$ (that is, $Y_1\to 1-Y_1$, $V_1\to -V_1$) when the particle crosses the top or bottom, and letting the particle bounce off the side walls elastically. Then, $\tilde{F}$ is the time-T mapping of this flow restricted to E.

Using the identification described above, any invariant set for $\tilde{F}$, including periodic orbits, chaotic attractors, and basin boundaries, can be extended to the whole phase space. If an orbit converges to an invariant set for $\tilde{F}$, the corresponding orbit for F has to converge to the extension of the invariant set in the whole space.

III. PARTICLE DYNAMICS

Figure 1 shows the projection onto the configuration space of the chaotic attractor for the mapping $\tilde{F}$ with the parameter values $A=3.2$, $W=0.8$, $R=1$, $k=2.72$, $\omega=\pi$ (this means that the forcing period is $T=2$). $W>0$, $R>2/3$ implies that the particles are lighter than the surrounding fluid. Numerical estimates of its average Lyapunov exponents are $\overline{\lambda_1}=0.030$, $\overline{\lambda_2}=-0.056$, $\overline{\lambda_3}=-3.119$, $\overline{\lambda_4}=-3.256$. The estimates of the box-counting dimension and the correlation dimension of the projection are 1.66 ± 0.02 and 1.48 ± 0.01, respectively. In addition to the chaotic attractor, there is a stable periodic orbit of period 7 on the hyperplanes defined by $Y_1=V_1=0$ and $Y_1=1$, $V_1=0$. Apparently, these are the only attracting invariant sets for this particular combination of parameter values.

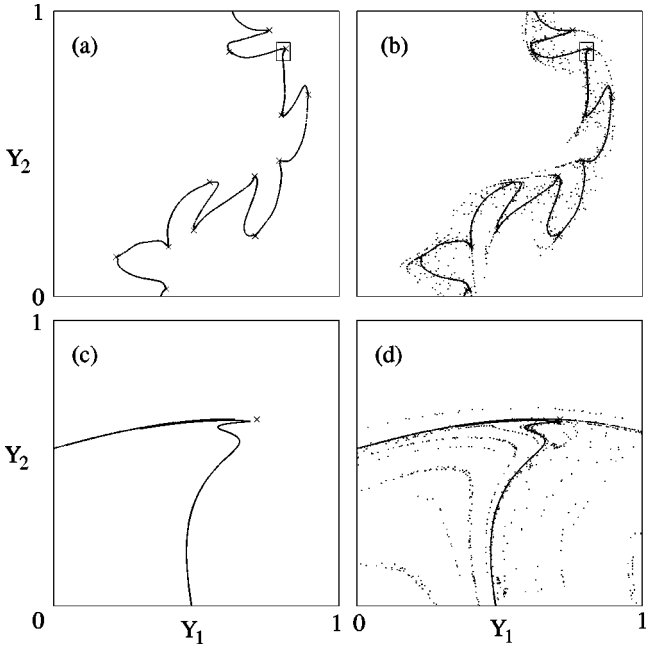

FIG. 2. Attracting sets (a) before ($k=2.6939$) and (b) after ($k=2.6940$) tangency. (c) and (d) show the blowup of the small rectangles shown in (a) and (b), respectively. The other parameters are $A=3.2$, $W=0.8$, $R=1$, $\omega=\pi$; and in each picture, a trajectory of length 30 000 is used after discarding the first 3000 iterations. The crosses indicate the unstable period 13 orbit involved in the tangency.

The chaotic attractor is created from a smooth torus, or an invariant curve that is shown in Fig. 2(a). As the parameter k is increased through the critical value ≈ 2.6939, the torus breaks up and turns into a chaotic attractor [Fig. 2(b)]. The closer k is to the critical value, the longer the trajectory spends time on the ''ghost'' of the torus, and it visits other parts of the chaotic attractor less often. The panels (c) and (d) in Fig. 2 show blow ups of the neighborhood of period 13 points to see the transition more clearly.

The essential element in the transition to chaos from the smooth torus is the period 13 orbit indicated in Fig. 2 as $\times$'s. It has three stable directions and one unstable direction. When k is below the critical value, the unstable manifold of this orbit does not intersect the stable manifold. The situation is schematically illustrated in Fig. 3(a). The smooth torus lies between the stable and unstable manifolds, as indicated by the dashed curve in the figure. As k is increased closer to the critical value, the unstable manifold gets more and more crumpled, and the torus gets crumpled as a consequence, since it is squeezed between the stable and unstable manifold. At the critical value of k, the torus, as well as the unstable manifold, is tangent to the stable manifold. If it is tangent at one point, it must be tangent at infinitely many points that accumulate on the periodic point because these points of tangency are on the stable manifold. As soon as k is

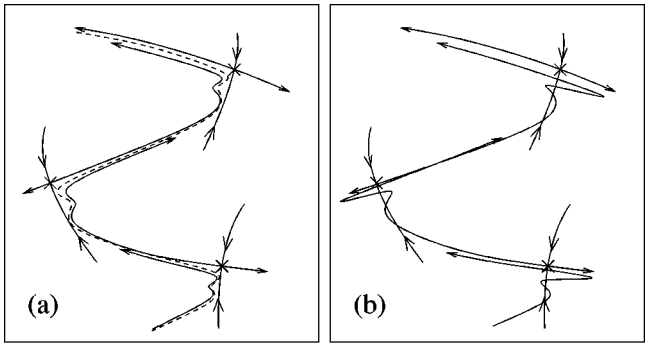

FIG. 3. Schematic drawing of stable and unstable manifolds of the period 13 orbit (a) before and (b) after the homoclinic tangency. The dashed curve in (a) is the smooth torus. The homoclinic tangency creates a chaotic attractor by breaking up the smooth torus.

above the critical value, the torus cuts across the three-dimensional stable manifolds of the period 13 orbits and it is stretched infinitely along the outer (and inner) branch of the unstable manifold [Fig. 3(b)]. This creates the fractal structure of the attractor, on which the dynamics exhibits exponential stretching and folding near the periodic points. Similar transition to chaos through the breaking of tori has been described in other systems [19,20].

IV. IMPLEMENTATION

Our finite-size particles are, however, active. Initially, we consider a catalytic, $A+B\rightarrow 2B$, type of activity. For the implementation of the active process, we consider, in the spirit of [1,3], a grid with resolution ε in the *physical* space. The difference between our work and the ones in previous studies is that the dynamics of the advected particles takes place both in the configuration and the velocity space, though the dynamics of the interface between the two reagents takes place only in the configuration space. The state of the system is completely determined by the positions and velocities of the B particles, since we regard the reagent A as the background fluid. Thus, in our model, the state of the system is represented by a list of B particles, each of which is associated with an ε cell and has a velocity vector.

Then, a single step of our process proceeds as follows. For each reagent particle B, we compute the trajectory of the particle with the initial position at the center of the corresponding ε cell and the initial velocity equal to the velocity associated with that particle. The integration is performed for time τ, and the ε cell that contains the particle's final position is now associated with that particle, and the final velocity of the particle becomes the new velocity associated with that particle. We do this for all B particles. If two or more particles from different cells move to the same cell, we simply keep the first particle in the cell, and remove all the other particles from the process. This choice of which particle does survive is completely arbitrary, and we could have, for example, chosen at random. This change would not affect the global dynamics of the distribution of the reagent B. After we evolved all the particles B for a time τ, we convert to B all the A cells within a distance σ of a B cell. For each cell converted to a B cell, a new B particle is created with the same velocity as its parent particle. The parameter σ is called the *reaction range*. This completes one cycle of our activity process.

The time period τ for which the particles are subjected to advection between successive reactions, is called the *reaction time lag*. Since we use the σ neighborhood for the reaction distance, the reaction front moves σ per time τ, so σ/τ is the reaction front velocity. The limit of $\sigma,\tau\rightarrow 0$ with σ/τ fixed, corresponds to the continuous reaction.

Since we initialize the trajectory of the particles for each cycle at the center of the ε cell, and since the trajectory does not necessarily arrive at the center of an ε cell, the size ε of these cells represents the error in computing the trajectory in our process.

The procedure in which we remove all but one particle when two or more particles end up in a single ε cell, can be regarded as another type of reaction, $B+B\rightarrow B$, called *coalescence*. This type of reaction itself plays an important role in biological population dynamics [21], and agglomeration phenomena in environmental physics, physical chemistry, and engineering [22–25]. We will discuss this in more detail in the Sec. VII.

For all the simulations in the following sections, we used the parameter values $A=3.2$, $W=0.8$, $R=1$, $k=2.72$, $\omega=\pi$ as in Fig. 1. This implies that the reagent particle B is a ''bubble,'' i.e., it is lighter than the surrounding fluid A and the buoyancy force pushes it upward.

V. CONTINUOUS FEEDING

Since the reagent B is lighter than the reagent A, all the B particles tend to $Y_2=\infty$ regardless of their initial positions. If we started with a distribution of particles in a vortex cell, all the particles eventually escape from that cell. This means that there is no bounded invariant set for the particle dynamics. The flow considered in [1,3,5] has the property that almost all trajectories escape the interaction region, but there are trajectories that spend very long time near the invariant chaotic saddle. If the reaction is faster than the escape rate of these trajectories, the system can sustain the reagent B indefinitely. In our case, however, we need to keep feeding the reagent B in order to sustain the reagent indefinitely, because the particle dynamics does not have any bounded invariant set.

Consider the infinite array of vortex cells with reagent B being fed at a point P. Numerically, we implement this by inserting a new particle at the point P every $\Delta t=0.02$ (period of the flow $T=2$). If the reagent B were inactive, the particles simply line up on the streak line from the point P. For an active reagent B, however, it covers the streak line with larger and larger thickness further up the vortex array, because at every time τ, strips of thickness σ are added on both sides of the streak line, due to the reaction. Figure 4 shows a snapshot of the distribution of the reagent B at $t=216$ with the time lag $\tau=6$.

For simplicity, let us consider the case where τ is an in-

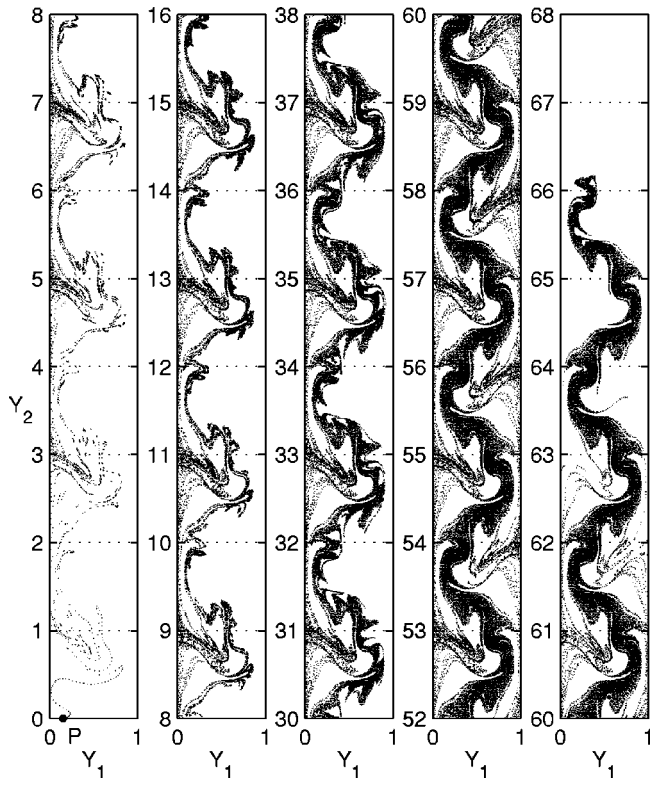

FIG. 4. A snapshot of the distribution of the particles B at $t=216$ with continuous feeding at the point P. The time lag $\tau=6$, the resolution $\varepsilon=0.01$, and reaction range $\sigma=0.01$ are used.

teger multiple of the period $T(=2)$ of the flow field, i.e., $\tau=nT$. Then, the advection of the reagent B in a single step is represented by the nth iterated map F^n. Although there is no bounded attractor for F, the orbits for F converge to the sets constructed by extending the attracting sets for the mapping $\tilde{F}$ to the entire phase space using the identification described in Sec. II. Hence, an orbit in the full phase space converges to the extension of either the chaotic attractor or the period 7 orbit in the hyperplane $Y_1=V_1=0$, shown in Fig. 1.

After injecting the reagent B for time τ, the reagent B forms a curve from the point P to its image $F^n(P)$ under the mapping F^n. If we continue injecting the reagent B, the image of this curve under F^n is added to the curve. The entire streak line can be constructed by adding the higher and higher iterates of the original curve in this fashion.

The streak line for our system takes a very complicated form, not only because of the chaotic attractor, but also because of the basin boundary between the chaotic attractor and the periodic orbit. In order to see why it is complicated, let us look at the evolution of a line segment under $\tilde{F}$. In Fig. 5, we plot the images under $\tilde{F}^4$, $\tilde{F}^8$, $\tilde{F}^{12}$, $\tilde{F}^{16}$, and $\tilde{F}^{20}$ of a line segment shown in the middle of panel (a). Images under F are similar except that it would extend through the whole space instead of winding around in E (recall the boundary at the top and the bottom are identified with a reflection about the line $Y_1=1/2$). There are two kinds of attractors for the mapping $\tilde{F}$, the chaotic attractor and the period 7 orbit on the hyperplane $Y_1=V_1=0$. Since the segment straddles the

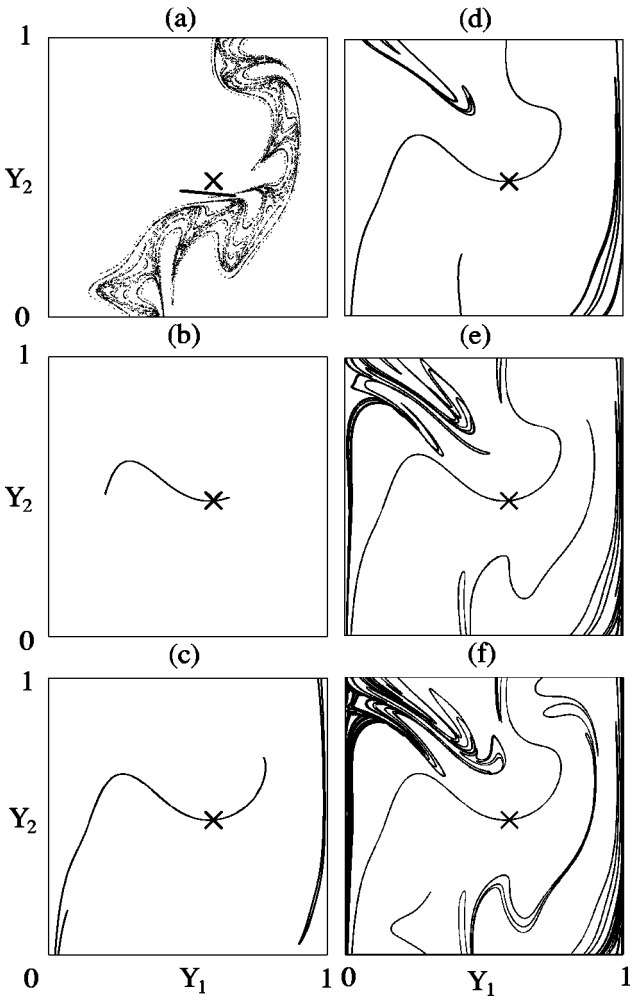

FIG. 5. Panels (a)–(f) show images of a straight line segment in panel (a) under (b) $\tilde{F}^4$, (c) $\tilde{F}^8$, (d) $\tilde{F}^{12}$, (e) $\tilde{F}^{16}$, and (f) $\tilde{F}^{20}$. The cross in each panel indicates a period 4 point lying in the basin boundary surface. The chaotic attractor is also shown in panel (a) for reference.

boundary of the basins of the chaotic attractor and the periodic orbit, some points on the segment go to the chaotic attractor, and others go to the periodic orbit. Thus, the segment is stretched quite a bit under the mapping, effect of which can be seen readily in Fig. 5.

A cross in Fig. 5 is located at one of the unstable period 4 points on the basin boundary surface. We used the method known as the basin straddle trajectories with Proper Interior Maximum (PIM) triple refinement method [26] to compute the trajectories on the basin boundary and found that trajectories on the boundary are attracted to this period 4 orbit. A point on the segment in Fig. 5 converges to the periodic orbit, and hence the entire segment converges to the *unstable* manifold of the same periodic orbit. One branch of the segment converges to the chaotic attractor, and the other connects to the stable period 7 orbit in the hyperplanes $Y_1=V_1=0$ and $Y_1=1$, $V_1=0$, while being stretched and folded. By simply extending these images to the whole space instead of winding around in E, the streak line exhibits the same intricate structure as long as the initial segment [from the injec-

tion point P to its image $F^n(P)$] of the streak line straddles the basin boundary. In fact, the intricate, fractal form implies that there must be infinitely many unstable periodic orbits on the boundary who provide the skeleton of a chaotic saddle. The streak line traces out the unstable manifold of this saddle, which is, however, numerically indistinguishable from that of the period 4 orbit.

Now we consider the reaction that takes place every time lag τ. Due to the reaction, the more often the initial segment is iterated, the thicker it becomes. Let S_0 denote the initial segment of the streak line connecting the point P to $F^n(P)$ and ε_0 be the average width of the coverage (ε_0 on each side of S_0) by the reagent B over this segment S_0. Let $S_i = F^{ni}(S_0)$ be the ith iterate of S_0 and ε_i be the average width of the coverage by the reagent B over the segment S_i. Then the reagent B covers the set $\cup_{i=0}^{\infty} S_i$ in the limit $t \to \infty$.

Note that the mapping F^n shrinks the width of the coverage of S_i at the rate λ_i, the weakest local contraction rate. Also note that the reaction can be regarded as adding strips of width σ on both sides of the existing strip of the reagent B along S_i. Thus, the recursive relation for the average width ε_i of the coverage of S_i by the reagent B is

$$\varepsilon_{i+1} = e^{\lambda_i \tau}(\varepsilon_i + g\sigma), \tag{8}$$

where $\lambda_i < 0$ is the the average weakest local contraction rate along S_i and g is a geometrical factor that takes into account the fact that the strips are not exactly straight line segments and that they might overlap one another ($g=2$ if there were no overlaps). If λ_i approaches a limiting value $\lambda^* < 0$, the average width should approach the corresponding limiting value ε^*. By substituting $\varepsilon_i = \varepsilon^*$, $\lambda_i = \lambda^*$ into Eq. (8) and solving for ε^*, we get

$$\varepsilon^* = \frac{g\sigma}{e^{-\lambda^*\tau} - 1}, \tag{9}$$

which is the asymptotic width of the coverage of streak line by the reagent B. The limiting value λ^* should be the weakest contracting Lyapunov exponent on the chaotic attractor or on the chaotic saddle.

Now, the segments S_i get longer and longer under the mapping F^n, extending through more and more vortex cells. However, the local properties of F^n along S_i is the same if we consider the images of S_0 under $\tilde{F}^n$ instead. If we look at one of the cells 50–58 in Fig. 4 and compare them with Fig. 5, it is evident that the reagent B is covering the entire unstable manifold of the chaotic saddle.

In Fig. 6, we plot the number of particles in each vortex cell at $t = 60,108,156,204$. According to the above argument, the number of particles in a cell approaches an asymptotic value for $t \to \infty$ and $Y_2 \to \infty$, because the coverage by the reagent B in a cell takes on a stationary form, in which the inflow of the reagent from the cell below together with the reaction balances the outflow to the cell above. In Fig. 6, the number of particles drops to zero for higher vortex cells, exhibiting transient behavior toward the stationary state. Although the number of particles quickly becomes too large and makes the simulation with continuous feeding difficult,

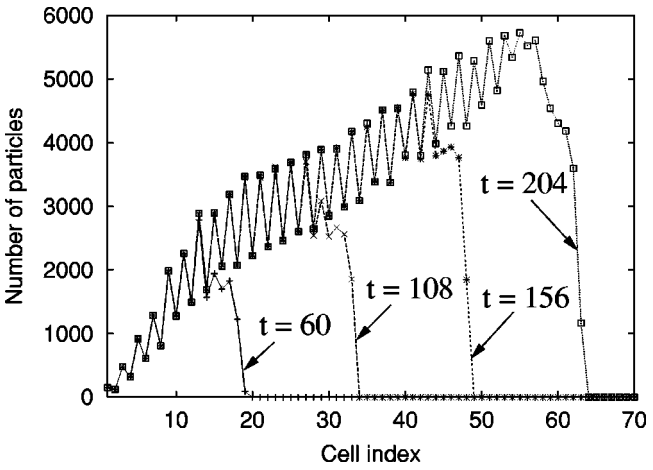

FIG. 6. The number of particles in each vortex cell for the snapshots at $t = 60,108,156,204$ in the case of continuous feeding. The resolution $\varepsilon = 0.01$, the reaction range $\sigma = 0.01$, and the time lag $\tau = 6$ are used. The times are indicated in the graph.

the asymptotic state can be analyzed by considering the stationary state under the mapping $\tilde{F}$ instead of F. We pursue this in the following section.

VI. CLOSED SYSTEM

We have seen in the preceding section that, in the limit of $t \to \infty$ and $Y_2 = \infty$, the distribution of reagent B in a vortex cell reaches a steady distribution. To analyze this further, we consider the time evolution of the distribution in the closed system, i.e., the time evolution under the advection dynamics given by the mapping $\tilde{F}$. Recall that the mapping $\tilde{F}$ is defined on the unit square, and the boundary condition on the edges of the square for the corresponding flow is periodic boundary with a reflection at the top and the bottom, and elastic collision with both side walls. We have two attractors, the chaotic attractor shown in Fig. 1, and the period 7 orbit lying in the planes $Y_1 = V_1 = 0$ and $Y_1 = 1$, $V_1 = 0$. The particles converge to one of the two attractors for almost all initial conditions.

Even though the system is closed in the sense that there is no escape of particles, the dynamics of the reaction always finds a stationary state. Figure 7 shows examples of snapshots of the distribution of the particles in the stationary states for different values of the time lag τ. They represent three distinct regimes in the τ-parameter space for which the system exhibits qualitatively different stationary states. For small values of τ up to about 8, the distribution of the particle seems to be smooth over the entire square. In this case, the reaction is fast compared to the contraction to the chaotic attractor and the escape from the chaotic saddle, resulting in filling up the configuration space with a smooth distribution. For large values of τ more than about 33, the distribution is concentrated on the chaotic attractor because of the dominance of the contraction over the reaction. For the intermediate values, the particles are distributed along the chaotic attractor and the unstable manifold of the chaotic saddle on the basin boundary. In this situation, the reaction is just slow

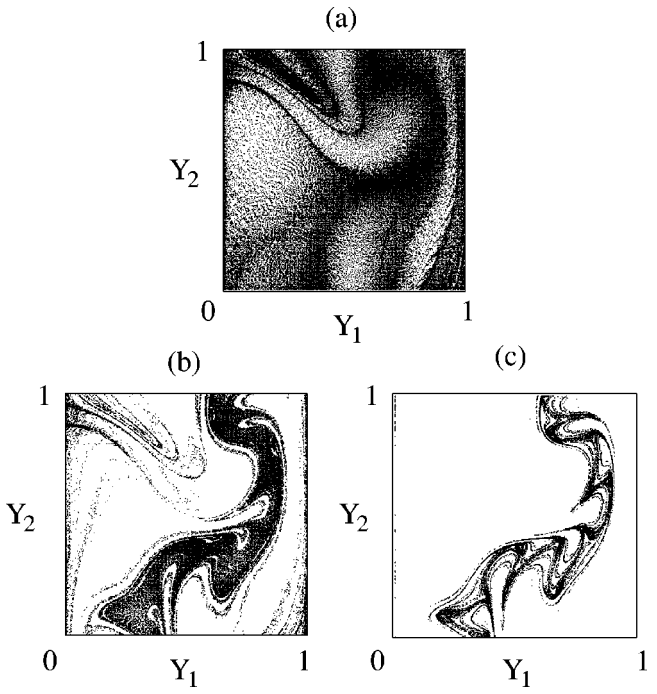

FIG. 7. The distribution of the reagent B in the steady state after 20 reaction cycles for (a) $\tau=8$, (b) $\tau=20$, (c) $\tau=50$, under the map $\tilde{F}$. We use $\varepsilon=\sigma=0.02$, which means that the resolution of the images is 157×157.

enough to prevent the reagent B from filling up the space, but not slow enough to be completely dominated by the contraction.

It is worthwhile to mention here that these images in Fig. 7 are the snapshots at multiples of the period $T=2$ of the background flow. The distribution of the reagent B actually changes with time. The fact that the system falls into a stationary state means that the evolution of the distribution is synchronized with the surrounding periodic flow field.

The reason for the system achieving a stationary state is the competition between phase volume contraction due to dissipation and expansion due to the activity of the reagent B. In the previous studies where open chaotic flows were considered [1,3,5], the escape from the chaotic saddle balanced the production of reagent B to achieve the stationary state. A simple replacement of the escape with the contraction in the particle dynamics allows us to derive a formula for the area covered by the reagent B in the stationary state.

We derive the formula here in a similar fashion as in [3,5]. Let $2>D_1>1$ be the information dimension of an invariant set (chaotic attractor or the saddle) of the system. The number of boxes of size ε needed to cover typical (with respect to the natural measure on the set) points of the invariant set scales as $\sim\varepsilon^{-D_1}$. If the set is covered with strips of width ε^* in Eq. (9), the area covered by these ε boxes scales as $\sim\varepsilon^{2-D_1}$ for ε not smaller than ε^*. In particular, by taking $\varepsilon=\varepsilon^*$, we have

$$\mathcal{A}^*(\tau)=\mathcal{H}\left(\frac{g\sigma}{c^{-\lambda^*\tau}-1}\right)^{2-D_1}, \tag{10}$$

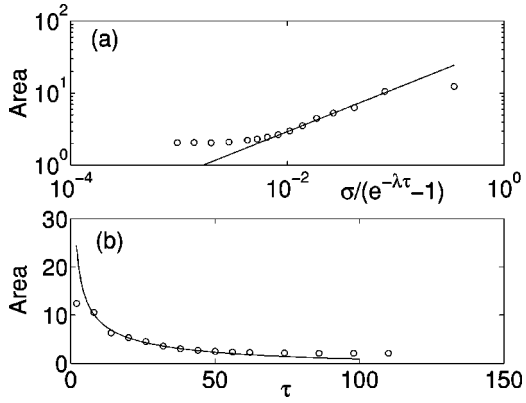

FIG. 8. The dependence of the area covered by the reagent B on the time lag τ, under the map $\tilde{F}$. We used $\varepsilon=\sigma=0.02$. The continuous curve is a fit according to Eq. (10) taken with $\lambda^*=-0.056$, the value on the attractor, and with $D_1=1.4$, $\mathcal{H}=45.9$.

where the prefactor $\mathcal{H}$ is called the Hausdorff measure of the invariant set. The formula has the same form as that of [3], except that here the escape rate is replaced by the average of the weakest local Lyapunov exponent $-\lambda^*$.

By inserting the relation $\varepsilon_i=(\mathcal{A}_i/\mathcal{H})^{1/(2-D_1)}$ into Eq. (8), one can also derive the recursion relation for the area $\mathcal{A}_i$ covered by the reagent B as

$$\mathcal{A}_{i+1}=e^{\lambda_i(2-D_1)\tau}[\mathcal{A}_i^{1/(2-D_1)}+g\sigma\mathcal{H}^{1/(2-D_1)}]^{2-D_1}. \tag{11}$$

Taking the limit of continuous reaction $(\tau,\sigma-0)$, we get

$$\dot{\mathcal{A}}=\lambda^*(2-D_1)\mathcal{A}+vg(2-D_1)\mathcal{H}^{1/(2-D_1)}\mathcal{A}^{-\beta}, \tag{12}$$

where $v=\sigma/\tau$ is the finite reaction front velocity, and $\beta=(D_1-1)/(2-D_1)$. This equation is also singular as the one in [3,5]. Note that $\lambda^*(2-D_1)<0$ because of the negativity of λ^*. Thus the first term in Eq. (12) describes the loss due to contraction (dissipation) while the second one represents the gain due to the reaction.

Figure 8 shows the τ dependence of the area $\mathcal{A}^*(\tau)$ from the simulation. The panel (a) shows the log-log plot of the area against $\sigma/(e^{-\lambda^*\tau}-1)$ that according to Eq. (10), reveals a straight line with slope equal to $2-D_1$. Here we used $\lambda^*=-0.056$, the weakest contracting Lyapunov exponent on the chaotic attractor. The circles lie on a straight line fairly well in a range of intermediate values of τ. The least square fit in this range results in the slope of about 0.6, which translates to $D_1\approx1.4$. Panel (b) shows the plot of the area against τ along with a curve corresponding to the least square fit from panel (a).

The box-counting dimension D_0 and the correlation dimension D_2 of the chaotic attractor are 1.66 ± 0.02 and 1.48 ± 0.01, respectively. The information dimension D_1 of the chaotic attractor lies between D_0 and D_2. In fact, according to the Kaplan-Yorke conjecture, $D_1=1-(\lambda_1/\lambda_2)\simeq1.53$. We have a small discrepancy with the above simulation on the dependence of the area of coverage. This is due to the fact that the reagent is covering not only the chaotic attractor, but also the unstable manifold of the chaotic saddle

on the basin boundary, as is seen in Fig. 7. We suspect that the values of λ^* and D_1 are different on these two invariant sets, and this explains the discrepancy.

As mentioned above, around $\tau=8$, there is a transition from a smooth distribution to a filamental distribution. This is similar to the smooth-filamental transition described in [2,4]. A difference from them is that we consider herewith an autocatalytic reaction instead of a linear decay reaction with source field. Nevertheless, some features such as direction dependent Hölder exponents (smooth distribution in one direction and singular in another) seem to be present in our system as well.

Also worth noticing is the so-called *emptying transition* [3] at around $\tau=33$. In the steady state for $\tau \lesssim 33$, the reagent B is distributed over the unstable manifold of the chaotic saddle as can be seen in Fig. 7(b). However, as τ is increased, less and less particles stay on the unstable manifold, until no particles remain in the neighborhood of the manifold for $\tau \gtrsim 33$. The contraction due to the escape of the particles from the chaotic saddle along its unstable manifold is no longer balanced by the production due to the reaction in this range of the phase space.

VII. COALESCENCE OF PARTICLES

As we explained in Sec. IV, our model includes another type of reaction, $B+B \rightarrow B$, which can be regarded as the coalescence of particles. Suppose that the particles represent a type of plankton that reproduces if there is enough food in the neighborhood, but dies if there are too many others and not enough food. Thus, the coalescence $B+B \rightarrow B$ can be thought of as the result of the competition for food.

This type of process with no other type of reaction in the system is interesting in its own right, and it was considered in [27]. We will summarize the results from [27] and describe an additional result in this section.

We consider the process consisting of two steps: the advection under the flow on the phase space E with appropriate boundary conditions and the reaction of the coalescence type. Regardless of the value of τ, the dissipation in the dynamics of the particles makes the distribution of the particles more and more concentrated on the attracting sets of the mapping $\tilde{F}$ as time elapses, because there is no production of new particles in the system. The number of particles can only decrease. We may focus only on the chaotic attractor, because the particles attracted to periodic orbits quickly collapse onto a fewer number of particles (only as many as the period of the orbit).

Once most of the particles come close to the chaotic attractor, the advection dynamics mixes the particles around within the neighborhood of the attractor. The mixing tends to make particles come within the reaction range and so it drives the decay of the number of the remaining particles in the system. Our simulation, in which we used a random initial distribution of the particles on the attractor according to its natural measure, consistently shows that the decay follows the power law t^{-1} regardless of the value of the time lag τ. The decay of the particle density (the number of particles divided by the initial number of particles) for typical runs of the simulation is shown in Fig. 9 (the $\tau=2$ case with $+$'s and the $\tau=10$ case with $\times$'s).

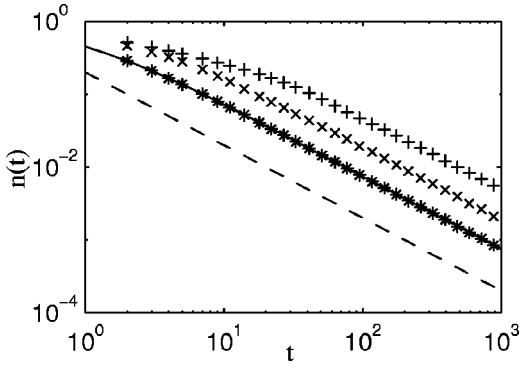

FIG. 9. The time evolution of the particle density for $\tau=2$ ($+$ symbols) and $\tau=10$ ($\times$ symbols). The stars ($*$) correspond to the random-shuffling model using the natural measure on the attractor, and the continuous line was computed from Eq. (13). The dashed line is the reference line with slope -1.

In order to understand such results, we approximate the entire process with a *random-shuffle* model. Recall that if the dynamics on the attractor is strongly mixing, the natural measure of an ε cell that intersects the attractor can be regarded as the probability for a typical trajectory on the attractor to hit the ε cell. With this analogy in mind, we consider the following model. Take the same number of balls as the number of particles in the system. For each ball, randomly choose an ε cell where we put the ball in, with the probability of choosing an ε cell equal to the natural measure of that cell. If there is another ball in that ε cell, the extra ball is discarded. Doing this for all the balls, at the end we will end up with fewer balls in the cells. This completes a single step of the process. Such a process can be simulated on a computer as well, using a random number generator, and a typical run of such a simulation is also shown in Fig. 9, with stars ($*$).

Simplicity of the model allows us to rigorously compute the evolution equation for the number of balls (B particles). Suppose we have n balls initially. Let $p(n,k)$ be the probability that the number of balls is k after one step of the process. $p(n,k)$ can be computed in the following way. The probability that n_1 balls are in i_1th box, n_2 balls are in i_2th box, $\ldots$, n_k balls are in i_kth box is

$$\frac{n!}{n_1!n_2!\cdots n_k!}p_{i_1}^{n_1}p_{i_2}^{n_2}\cdots p_{i_k}^{n_k}.$$

Summing this over all $1 \leqslant n_1, \ldots, n_k \leqslant n$ such that $n_1+\cdots+n_k=n$, and using multinomial formula, we get

$$\sum_{n_1=1}^{n-k+1}\cdots\sum_{n_k=1}^{n-k+1}\frac{n!}{n_1!n_2!\cdots n_k!}p_{i_1}^{n_i}p_{i_2}^{n_2}\cdots p_{i_k}^{n_k}\delta_{n_1+\cdots+n_k,n}$$

$$=\frac{n!}{(n-k)!}\int_0^{p_{i_1}}dx_1\cdots\int_0^{p_{i_k}}dx_k(x_1+\cdots+x_k)^{n-k}$$

$$=\sum_{m=1}^{k}(-1)^{k-m}\sum_{L_m\subset I_k}(p_{l_1}+\cdots+p_{l_m})^n,$$

where $I_k=\{i_1,\ldots,i_k\}$ and the last summation is over all subset $L_m=\{l_1,\ldots,l_m\}$ of I_k. The second equality can be proved by induction in k. $p(n,k)$ is obtained by summing this over all possible combinations of $i_1,\ldots,i_k$:

$$p(n,k)=\sum_{i_k}\sum_{m=1}^{k}(-1)^{k-m}\sum_{L_m\subset I_k}(p_{l_1}+\cdots+p_{l_m})^n$$
$$=\sum_{m=1}^{k}(-1)^{k-m}\binom{N-m}{k-m}\sum_{L_m\subset\{\overline{1,N}\}}(p_{l_1}+\cdots+p_{l_m})^n.$$

The last equality is due to the fact that a particular combination L_m appears $\binom{N-m}{k-m}$ times in the summation. By plugging this into the usual definition of the expected value of k and reducing the resulting expression using combinatorial equalities, we get

$$\sum_{k=1}^{n}kp(n,k)=\cdots=N-\sum_{i=1}^{N}(1-p_i)^n.$$

The equation for the one-step evolution of the number density can be derived using the above. Here the number density $n(t)$ of the particles at time t refers to the number of particles at time t divided by the initial number N of particles at time zero. We take N to be the number of ε cells that intersect the attractor, i.e., we distribute particles uniformly over the attractor at time 0. The evolution equation can then be written as

$$n(t+1)=1-\frac{1}{N}\sum_{i=1}^{N}(1-p_i)^{Nn(t)}, \tag{13}$$

where p_i is the natural measure of the ith ε cell. Since p_i's are small, we may expand the terms in the summation on the right-hand side to obtain

$$\frac{dn}{dt}=-C[n(t)]^2,$$

where $C=(N/2)\Sigma_{i=1}^{N}p_i^2$. The solution of this equation is simply $(Ct+1)^{-1}$ and it scales as t^{-1}. The number C is related to the dimensions of the attractor by $C=\varepsilon^{D_2-D_0}$, where D_2 is the correlation dimension and D_0 is the box-counting dimension [28]. Using these, we find that the number density decay follows the scaling

$$n(\varepsilon,t)\sim\varepsilon^{-D_2}t^{-1}. \tag{14}$$

We verify this numerically as following. We measure the decay of the number density for different values of ε. For each fixed t, we find the scaling exponent $-\gamma$ with ε. In Fig. 10, we plot these scaling exponents as a function of time t. One can see that, except for the transient region (small t) and the region where $n(\varepsilon,t)$ is too small (large t), exponents are close to the numerically computed value of $D_2=1.48$ of the correlation dimension of the attractor. For the calculation of exponents $-\gamma$, we use seven values of ε in the interval [0.005,0.056] equally spaced in the logarithmic scale.

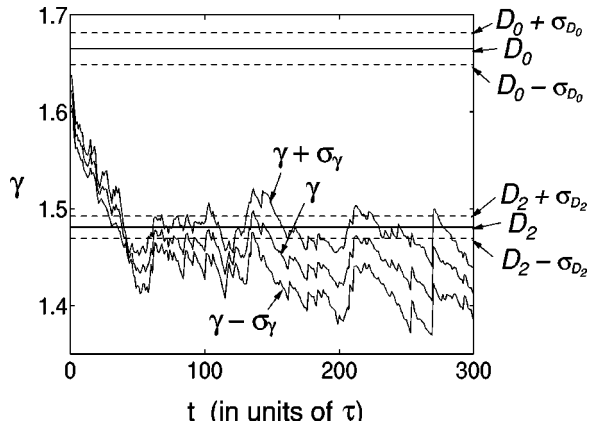

FIG. 10. Scaling exponent γ for the number density, in the case of the closed system. σ_γ is the estimated standard deviation from the least squares fit. D_0,D_2 are the box-counting and correlation dimensions of the chaotic attractor, respectively, and σ_{D_0} and σ_{D_2} are the corresponding standard deviations for the least squares fit for γ. $D_0\approx1.66$, $D_2\approx1.48$, $\sigma_{D_2}=0.02$, and $\sigma_{D_2}=0.01$. Here we took $\tau=50$.

Our model is consistent [27] with the Smoluchowski equation from the theory of the agglomeration reactions $B_i+B_j\rightarrow B_{i+j}$ [23,24]. It is important to notice that these two results independently verify our theory based on the random-shuffling model.

VIII. CONCLUSIONS

We have analyzed in this work the dynamics of autocatalytic reaction of small, but finite-size particles in the time-periodic cellular vortex flow field. The inertia of the active particles makes their dynamics dissipative and makes it possible to have chaotic attractors with fractal structure in their spatial component.

For the particular parameter values of the particle dynamics that we considered, a chaotic attractor and a stable periodic attractor coexist. The coexistence of the two attractors turns out to be the reason why a typical streak line has a complicated structure. Significant amount of stretching takes place along a streak line, because it passes through a chaotic saddle lying on the basin boundary surface of the two attractors, whose neighborhood is stretched along its unstable manifold.

By continuously injecting the reagent B, which goes through the reaction $A+B\rightarrow2B$ at the interface with the background fluid A, the streak line is covered by the reagent B with greater and greater thickness as the reagent traces further up the streak line. Due to the contraction by the particle dynamics, the average thickness approaches the asymptotic value.

To analyze the asymptotic distribution for $Y_2\rightarrow\infty$, we introduced the appropriate boundary conditions on the phase space E and considered the active dynamics. We showed that for intermediate values of the time lag τ, the coverage by the reagent B in the stationary state follows similar formula as in the case of ideal tracers, except that the escape rate from the chaotic saddle is replaced by the weakest contracting average

Lyapunov exponent on the chaotic attractor and on the chaotic saddle on the basin boundary. For smaller values of τ, there occurs an interesting transition from singular distribution of particles to a smooth one. This is similar to the smooth-filamental transition studied in [2,4], but they have only studied the linear decay reaction with source field. Further investigation into the relationship to their system is a topic of future work.

The problem we studied in this paper is much more complex than the corresponding problem with ideal tracers, mainly due to the fact that it possesses attractors and that more than one attractors coexist. Consequently, we observe different regimes in the τ parameter space. Since the flow is closed, the emptying transition observed in the case of open flows occurs in a different context, as emptying *from a chaotic saddle to an attractor*.

Although, this paper provides the description of chemical activity of inertial particles under chaotic advection, it is worth comparing the passive properties of the model with a recent approach of Balkovsky, Falkovich, and Fouxon [29]. These authors consider *random* hydrodynamical flows and weak inertia effects ($A \gg 1$ in our notation) on advection. Nevertheless, they find a tendency of clustering, which is consistent with the weakly dissipative character of the particle dynamics in their limit. The same effect is much stronger in our case, where the inert tracer problem ($A=\infty$) is nonchaotic, but at order 1 values of the inertia parameter A, large scale chaotic attractors appear. In both approaches, clear accumulation of particles takes place. Therefore, we conclude that enhancement of chemical activity can be expected in random flows, too, due to particle inertia.

Finally, in the case of coalescence reaction, we have shown, for sufficiently slow reactions, that the decay of number density follows a universal scaling law $\sim t^{-1}$. This agrees well with our analytical result using a random-shuffle model. Furthermore, we have also verified the scaling with the reaction range predicted from our analytical result through a direct numerical simulation.

ACKNOWLEDGMENTS

Z.T. was supported by the U.S. Department of Energy under Contract No. W-7405-ENG-36. Support from the Hungarian Science Foundation (OKTA T032423), the US-Hungarian Joint Fund (Project No. Int. 501) and the MTA/OTKA/NSF Fund (Project No. Int. 526) is acknowledged. C.G. was supported by FAPESP, CNPq, and ONR.

[1] Z. Toroczkai, G. Károlyi, Á. Péntek, T. Tél, and C. Grebogi, Phys. Rev. Lett. **80**, 500 (1998).
[2] Z. Neufeld, C. López, and P. H. Haynes, Phys. Rev. Lett. **82**, 2606 (1999).
[3] G. Károlyi, Á. Péntek, Z. Toroczkai, T. Tél, and C. Grebogi, Phys. Rev. E **59**, 5468 (1999).
[4] Z. Neufeld, C. López, E. Hernández-García, and T. Tél, Phys. Rev. E **61**, 3857 (2000).
[5] T. Tél, G. Károlyi, Á. Péntek, I. Scheuring, Z. Toroczkai, C. Grebogi, and J. Kadtke, Chaos **10**, 89 (2000).
[6] I. Scheuring *et al.*, Freshwater Biol. **45**, 123 (2000); G. Károlyi *et al.*, Proc. Natl. Acad. Sci. U.S.A. **97**, 13 661 (2000).
[7] S. A. Spall and K. J. Richards, Deep-Sea Res., Part I **47**, 1261 (2000).
[8] A. P. Martin, J. Plankton Res. **22**, 597 (2000).
[9] A. Mahadevan and D. Archer, J. Geophys. Res., [Oceans] **105**, 1209 (2000).
[10] A. P. Martin and K. J. Richards, Deep-Sea Res., Part II **48**, 757 (2001).
[11] H. Malchow and S. V. Petrovskii, *Numerical Study of Plankton-Fish Dynamics in a Spatially Structured and Noisy Environment*, Ecological Modelling (unpublished).
[12] O. Paireau and P. Tabeling, Phys. Rev. E **56**, 2287 (1997).
[13] C. López *et al.*, Phys. Chem. Earth **26**, 313 (2001); C. López *et al.*, Chaos **11**, 397 (2001).
[14] M. R. Maxey, Phys. Fluids **26**, 883 (1983).
[15] M. R. Maxey, Phys. Fluids **30**, 1915 (1987).
[16] L. Yu, C. Grebogi, and E. Ott, in *Nonlinear Structure in Physical Systems*, edited by L. Lam and H. C. Morris (Springer-Verlag, New York, 1990), pp. 223–231.
[17] T. R. Auton, J. C. R. Hunt, and M. Prud'homme, J. Fluid Mech. **197**, 241 (1988).
[18] M. J. Manton, Boundary-Layer Meteorol. **6**, 487 (1974).
[19] J. H. Curry and J. A. Yorke, in *The Structure of Attractors in Dynamical Systems*, Lecture Notes in Mathematics Vol. 668 (Springer-Verlag, New York, 1978).
[20] P. M. Battelino, C. Grebogi, E. Ott, and J. A. Yorke, Physica D **39**, 299 (1989).
[21] T. Czárán, *Spatiotemporal Models of Population and Community Dynamics* (Chapman & Hall, London, 1998).
[22] *Topics of Current Aerosol Research*, edited by G. Hidy and J. Brock (Pergamon, New York, 1971).
[23] M. von Smoluchowski, Z. Phys. **17**, 557 (1916).
[24] E. Ben-Naim and P. Krapivsky, J. Phys. A **33**, 5465 (2000).
[25] P. Krapivsky and E. Ben-Naim (unpublished).
[26] C. Grebogi, H. E. Nusse, E. Ott, and J. A. Yorke, in *Dynamical Systems*, edited by J. C. Alexander, Lecture Notes in Mathematics Vol. 1342 (Springer-Verlag, Berlin, 1988), pp. 220–250.
[27] T. Nishikawa, Z. Toroczkai, and C. Grebogi, Phys. Rev. Lett. **87**, 038301 (2001).
[28] H. G. E. Hentschel and I. Procaccia, Physica D **8**, 435 (1983).
[29] E. Balkovsky, G. Falkovich, and A. Fouxon, Phys. Rev. Lett. **86**, 2790 (2001).